Asian Journal of Pharmaceutical Sciences 20 (2025) 101014

Available online at www.sciencedirect.com

ScienceDirect

journal homepage: www.elsevier.com/locate/AJPS

Short Communication

Efficient anticancer drug delivery using nano-colloids self-assembled with an unconventional amphiphile bearing pumpkin-shaped host molecule

Kyeng Min Park

Department of Biochemistry, Daegu Catholic University School of Medicine, 33 Duryugongwon-ro 17-gil, Nam-gu, Daegu, 42472, Republic of Korea

ARTICLE INFO

Article history:
Received 11 December 2023
Revised 20 November 2024
Accepted 27 November 2024
Available online 2 January 2025

Keywords:
Cucurbituril
Unconventional amphiphile
Self-assembly
Host-guest chemistry
Drug delivery

ABSTRACT

A new type of amphiphiles bearing macrocycle such as cucurbit[7]uril (CB[7]) spontaneously forms a nanomaterial in water, specifically vesicles (tACB[7] vesicles) with a positive surface charge, verified through various analytical techniques including TIRF, DLS and TEM. Functional validation not only reveals the accessibility of the CB[7] portal on these vesicles allowing CB[7]-based host-guest interactions with various functional guest molecules such as fluorescein isothiocyanate conjugated adamantylammonium and spermine (FITC-AdA and FITC-SPM, respectively) using confocal laser scanning microscopy, but also showcases the effective internalization of tACB[7] vesicles into cancer cells with the anticancer drug oxaliplatin (OxPt), as a guest to CB[7], through *in vitro* cell experiments. Hence, this study provides a blueprint to impart amphiphilic properties to CB[7] through synthetic design and highlights the potential of CB[7] derivatives as a new class of unconventional amphiphiles self-assembling into functional nanomaterials for advanced drug delivery.

1. Introduction

Nanocolloids, such as micelles and vesicles, that are spontaneously formed with amphiphiles have been exploited for various bioapplications, including delivery vehicles and imaging materials. Organic macrocycle derivatives, including calixarenes, cyclodextrins, pillararenes and cucurbiturils (CB), have emerged as a novel class of amphiphiles that are capable of host–guest chemistry-driven applications, such as sensing, imaging, and drug loading [1–3]. Among these, cucurbit[*n*]uril (CB[*n*], cyclized with *n* glycoluril units, $n = 5$–8, 10 and 13–15, in a hollow, pumpkin -like structure) are known to have distinct host–guest interaction with various hydrophobic drugs and bioactive molecules taking advantage of their rigid structure comprising a hydrophobic cavity and carbonyl fringed portals [1–8]. The functionalization issues of CB[*n*] have been addressed [9–14], and subsequently, it

E-mail address: kpark@cu.ac.kr
Peer review under responsibility of Shenyang Pharmaceutical University.

https://doi.org/10.1016/j.ajps.2024.101014

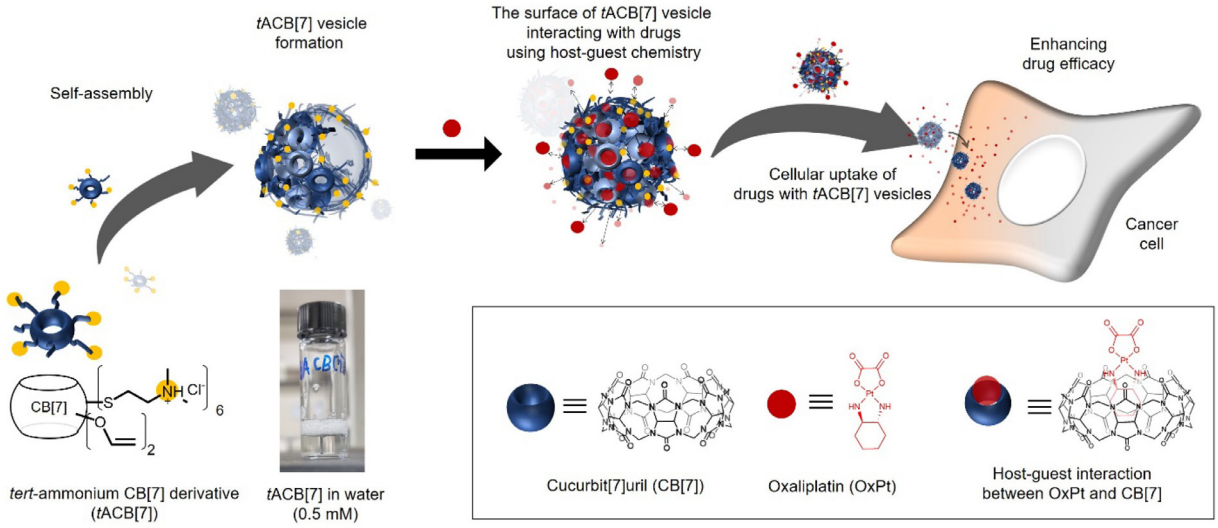

Fig. 1 – Self-assembly of *tert*–ammonium CB[7] (tACB[7]) and its cellular uptake with drugs using CB[7]-based host-guest chemistry and host-guest interactions of OxPt with CB[7].

has been exploited further as a platform for developing self-assembled nanomaterials, such as vesicles and nanoparticles. Initial investigations focused primarily on CB[6] derivatives owing to its availability in larger quantities compared with other CB[*n*], which is beneficial for developing various derivatives [15–17]. Subsequently, advancements in synthetic routes led to improvements in the yields of CB[7] and its derivatives [18–23], thus resulting in the synthesis of CB[7] derivatives with the unique ability to spontaneously form nanomaterials [24–29]. For example, monoallyloxylated CB[7], synthesized directly from monohydroxylated CB[7], can act as an amphiphile and form vesicles that respond to light stimuli and rupture, thus causing them to release a drug, such as doxorubicin, in cytosol [24]. Nanomaterials self-assembled with amphiphilic CB[7] derivatives are advantageous over CB[6]-based nanomaterials owing to the larger cavity of CB[7], which allows accommodation of a wider range of hydrophobic molecules, including drugs and bioactive agents [30–31]. Nevertheless, a CB[7] derivative that is intentionally designed to possess amphiphilicity has not been reported thus far, except for one whose amphiphilic nature was serendipitously discovered and which formed self-assembled vesicles [24].

Herein, we report a synthetic strategy to confer amphiphilicity to CB[7] by introducing hydrophilic groups, such as *tertiary* ammonium moieties, on its periphery and demonstrate the ability of the CB[7]-based amphiphile to spontaneously form vesicles having a positive surface charge in water. Furthermore, we demonstrate the internalization of the vesicles with their guest molecules into cancer cells (Fig. 1). Leveraging the unique host–guest interaction of CB[7], particularly its ability to form complexes with anticancer agents such as oxaliplatin (OxPt) [32–35], enhances the cytotoxic effect of the drug on cancer cells when treated concurrently with these vesicles. These findings not only offer a guideline for developing a new class of unconventional amphiphiles through deliberate synthetic design, but also highlight the potential utility of self-assembled nanomaterials composed of unique macrocyclic amphiphiles for drug delivery applications.

2. Materials and methods

2.1. *Material*

Acetone and diethyl ether were purchased from Samchun chemicals Co. Ltd. Republic of Korea. Methanol, DMSO, OxPt, Hoechst 33,258, methylthiazolyldiphenyl-tetrazolium bromide (MTT) and 2-(dimethylamino)ethanethiol hydrochloride were purchased from Sigma-Aldrich, USA. DMSO–d_6 was purchased from Cambridge Isotope Laboratories, USA. Cellulose ester (CE) membrane tubing having molecular weight cut-off (MWCO) 100–500 Da (Spectra/Por^{TM}) and regenerated cellulose (RC) membrane tubing having MWCO 3.5 kDa (SnakeSkin^{TM}) were purchased from Thermo Scientific, USA. A syringe filter (PTFE, 200 nm pores) was purchased from Millipore, USA. A hand mini-extruder and an extrusion membrane (100 nm pore size) were purchased from Avanti Polar Lipids, USA. Dulbecco's Modified Eagle Medium (DMEM) medium, fetal bovine serum (FBS) and penicillin-streptomycin (PS) were purchased from Gibco, USA. Phosphate buffered saline (PBS) was purchased from Welgene, Republic of Korea. Multi-allyloxylated CB[7], FITC-SPM and FITC-AdA were synthesized by following the previously reported procedure [11,15,24].

2.2. *Synthesis of* tertiary *ammonium conjugated CB[7] (tACB[7])*

To a solution of multi-allyloxylated CB[7] (20 mg, 12 µmol) in methanol (5 ml) in a quartz tube was added 2-(dimethylamino)ethanethiol hydrochloride (32 mg, 300 µmol). After degassing with N_2, the mixture was irradiated with

UV light (λ_{max} 254 nm) for 2 d Initially, the reaction mixture appeared turbid due to the poor solubility of allyloxylated CB[7] in methanol. However, as the reaction progressed, the solution became clear. After the reaction, the mixture was filtered through a syringe filter (PTFE, 200 nm pores) and the solvent was removed under reduced pressure, resulting in the formation of a viscous liquid. To remove any remaining unreacted allyloxylated CB[7], the liquid was dissolved in methanol and filtered through a syringe filter (PTFE, 200 nm pores). The filtrate was then transformed into solid precipitates upon the addition of diethyl ether. To remove residual unreacted *tert*–ammonium thiols, the precipitated solid was then washed with excess amount of acetone three times and dried *in vacuo*, followed by dialysis against water using a CE membrane tubing (MWCO 100–500 Da) to give tACB[7] (15 mg, 67%). The ^{1}H NMR peaks of the final product (0.5 mM) in DMSO–d_6 were assigned in Fig. 2C. Considering the same diffusion behavior of the CB[7] motif and thiol groups in the final product, exhibiting a smaller diffusion coefficient in the DOSY spectrum than those of the allyloxylated CB[7] and thiol, along with the prominent peak in the MALDI-TOF spectrum (Fig. S2), it becomes apparent that the predominant constituent in the product is the CB[7] derivative conjugated with six thiol groups.

2.3. Preparation of tACB[7] vesicles

A solution of tACB[7] (1.2 mg) in methanol (10 µl) in a round-bottom flask was subjected to vacuum drying to produce a tACB[7] film. DI water (1 ml) was then added to the film and vigorously shaken, followed by 1 h sonication to provide tACB[7] vesicles (0.5 mM). The solution of the vesicles was passed through a membrane (100 nm pore size) 21 times using a hand mini-extruder. Verification of the vesicles' size and morphological characteristics was accomplished by dynamic light scattering (DLS) and transmission electron microscopy (TEM), respectively (Fig. 3 and S4).

2.4. Preparation of FITC-AdA (or FITC-SPM) decorated tACB[7] vesicles

FITC-AdA or FITC-SPM (5 µg) was added to a solution of tACB[7] vesicles (0.5 mM; 1 ml). The resulting solution was gently shaken for 1 h at RT and dialyzed (MWCO 3.5 kDa) against water for overnight. Successful decoration of FITC-AdA on the surface of the vesicles was imaged by EM-CCD (Hamamatsu) installed in total internal reflection fluorescence (TIRF) microscopy system (Eclipse Ti-E, Nikon, 100x/N.A.1.49 objective lens). As a control, the same experiment was performed with CF (3 µg) instead of FITC-AdA (or FITC-SPM).

2.5. TEM, DLS and surface charge measurements

A drop of a vesicle solution (0.5 mM) in water was loaded on a 400 mesh carbon-coated copper grid and then gently blotted with a filter paper. The specimen was stained with a drop of uranyl acetate solution (0.5 wt% in water), incubated for 5 min, and gently blotted with a filter paper (Whatman). TEM images were recorded on a Titan G2 Cube 60–300 (FEI) with 80 kV acceleration voltage.

An aqueous solution of vesicles (0.1 mM) was placed in a quartz cuvette and the particle diameter was measured at a scattering angle of 90° (Litesizer 500, Anton Paar, 658 nm, 40 mW). The zeta potential of the vesicle solution was measured using an Omega cuvette (Anton Paar). Both DLS and the zeta potential measurements were conducted under the same conditions using a vesicle solution after treatment with OxPt (100 µM).

2.6. Critical assembling concentration measurement

The critical assembling concentration was determined via surface tension measurements and drop shape analysis using a 21 G needle at 25 °C and aqueous solutions containing varying concentrations (0.001–1 mM) of tACB[7]. A pendant drop was produced at the end of the needle and elongated by gravity and an image was taken immediately. The surface tension was calculated by analyzing the drop geometry in the image using the axisymmetric drop shape analysis method [36].

2.7. Confocal laser scanning microscope images of HeLa cells

HeLa cells were seeded in a 8-well confocal glass chamber at a density of 5×10^4 cells per well in 500 µl of a DMEM medium containing 10% FBS and 1% PS and incubated in a humidified 5% CO_2 atmosphere at 37 °C for 24 h The culture medium was replaced with 500 µl of a fresh one including FITC-AdA (or FITC-SPM) treated tACB[7] vesicles (0.05 mM) for 4 h at 37 °C, and then the cell culture medium was replaced with 500 µl PBS including Hoechst 33,258 (1 µg/ml) before incubated for an additional 15 min at 37 °C. The HeLa cells on in the confocal chamber were examined by a confocal laser scanning microscope (LMS900 with 40x/N.A. 1.2 Water immersion, Zeiss) with emission at 488 nm and 405 nm for FITC and Hoechst 33,258, respectively.

2.8. Cytotoxicity of tACB[7] vesicles against HeLa cells

HeLa cells were placed in a 96-well plate, with each well containing 1×10^4 cells in 200 µl DMEM medium supplemented with 10% FBS and 1% PS. Subsequently, the plate was incubated in a humidified 5% CO_2 atmosphere at 37 °C for 24 h The cell culture medium was then replaced with 200 µl fresh medium containing varying concentrations of tACB[7] vesicles (0.08–180 µM) and incubated for 24 and 48 h, respectively. Then, 20 µl of a methylthiazolyldiphenyl-tetrazolium bromide (MTT) solution (5 mg/ml) was added to each well and incubated for 4 h at 37 °C. After the incubation period, the medium was carefully removed. The purple, water-insoluble crystals formed by viable cells were then dissolved with 200 µl DMSO. The plates were gently agitated for 10 min to ensure complete dissolution of the crystals. The UV absorbance of the resulting solution in each well was measured at 590 nm using a multi-well plate reader (SpectraMax iD5, Molecular Devices). To quantify the results, the blank value was subtracted from each measurement, and the values were normalized against the control. This entire procedure was conducted in triplicate to calculate the

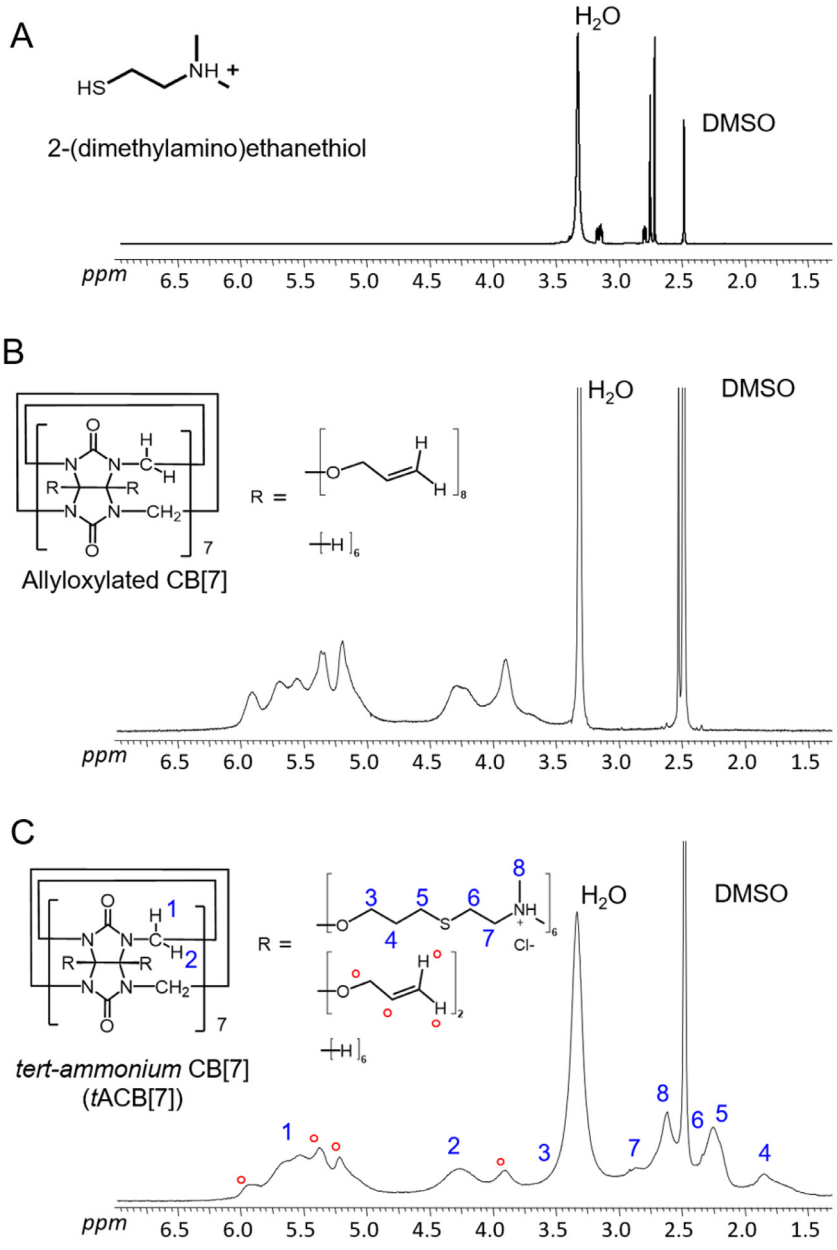

Fig. 2 – ^{1}H NMR spectra of (A) 2-(dimethylamino)ethanethiol (*tert*–ammonium thiol), (B) allyloxylated CB[7], and (C) tACB[7] in DMSO–d_6, before and after conjugation of *tert*–ammonium conjugation.

standard deviation. To evaluate the cytotoxicity of OxPt to HeLa cells upon treatment with CB[7] and the tACB[7] vesicles, the same experiment was performed using 24 and 48 h incubation of OxPt (0.8–150 μM), OxPt co-treated with CB[7] (10 μM), and OxPt co-treated with tACB[7] vesicles (10 μM), instead of using varying concentrations of tACB[7] vesicles.

3. Results and discussions

3.1. *Synthesis of tACB[7]*

In the design of the new CB[7]-derived amphiphile, the hydrophilic functionality was conjugated to a non-water-soluble CB[7] derivative. In this study, a CB[7] derivative with eight allyloxyl groups (on average) on its periphery, synthesized following a previous report[11] and a commercially available *tertiary* ammonium (*tert*–ammonium) thiol, 2-(dimethylamino)ethanethiol hydrochloride, were chosen. The conjugation reaction was carried out in methanol in a quartz tube through a thiol-ene photoreaction (λ_{max} = 254 nm). Although the initial reaction mixture appeared turbid owing to the limited solubility of the CB[7] derivative in methanol, it gradually became clearer as the reaction proceeded. After a 2-d reaction period, the reaction mixture was washed with diethyl ether and acetone, followed by dialysis against water using a cellulose ester (CE) membrane having 100–500 Da of MWCO to obtain the newly synthesized *tert*–ammonium conjugated CB[7] (tACB[7]) in a 67% yield. A comparison of the ^{1}H NMR (nuclear magnetic

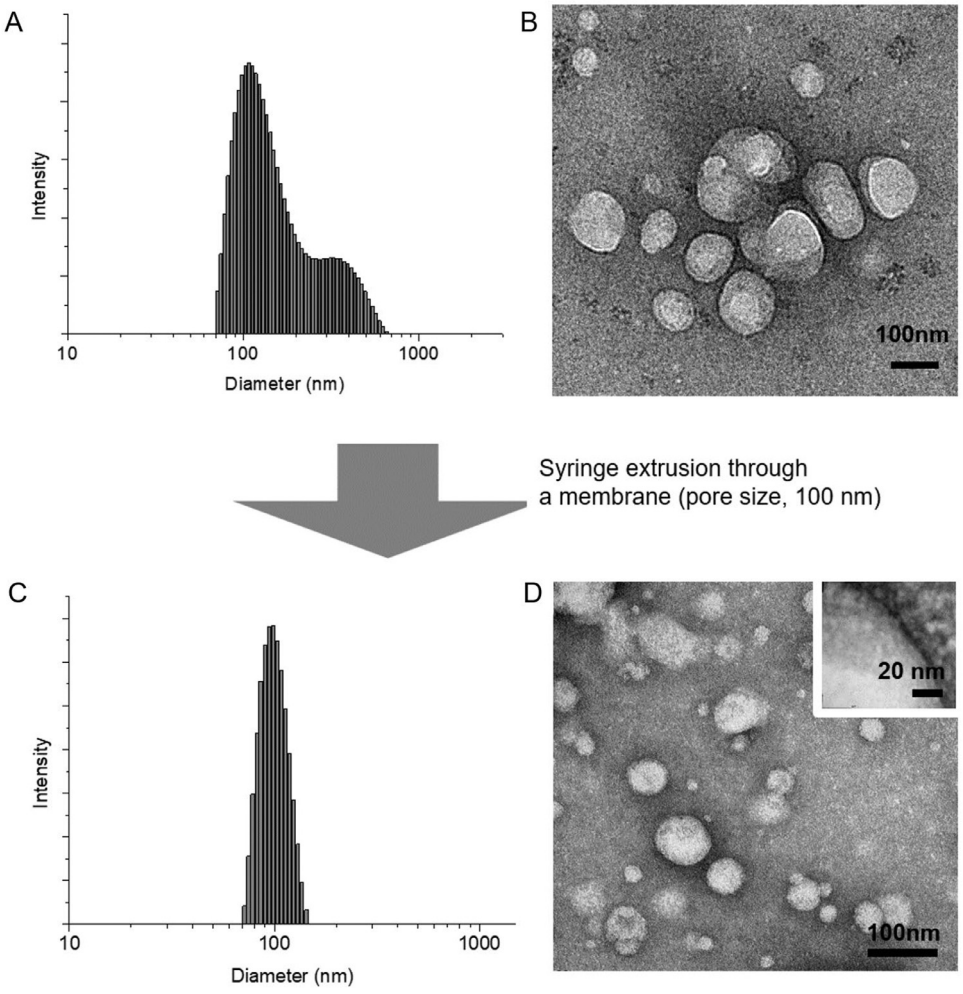

Fig. 3 – (A, C) DLS and (B, D) TEM of tACB[7] assemblies. The images are taken (A&B) before and (C&D) after repeated extrusion through a membrane having 100 nm pores.

resonance) spectra of the starting allyloxylated CB[7] (Fig. 2B) and purified product revealed that the appearance of proton peaks (6–8 in Fig. 2C) in the photoreacted product is attributed to the 2-(dimethylammonium)ethyl groups. Notably, the proton peaks in the photoreacted product are broader compared to those of the starting *tert*–ammonium thiol (Fig. 2A). This broadening indicates the conjugation of thiol to the rigid structure of the CB[7] motif, which has a short T2 relaxation time. Additionally, proton peaks corresponding to the unreacted allyloxyl groups were detected in the purified product, as indicated by the open circles in Fig. 2C. The combined analysis of the ^{1}H NMR spectroscopy (Fig. 2C) and MALDI-ToF mass spectrometry (Fig. S2B) results indicate that tACB[7] has six conjugated *tert*–amino groups on average, along with two unreacted allyloxyl groups. Diffusion-ordered NMR spectroscopy (DOSY) of tACB[7] revealed that all product peaks, except the solvent peaks (water and DMSO), had almost identical diffusion coefficients (see the grey area in Fig. S2). These coefficients are smaller than those of the unreacted allyloxylated CB[7] and *tert*–ammonium thiol (Fig. S2), indicating that tACB[7] is bigger than the starting reagents. Such a finding clearly demonstrates the conjugation of *tert*–ammonium thiols to the CB[7] derivative.

3.2. *Self-assembly of tACB[7] forming vesicles in aqueous solution*

The newly synthesized tACB[7] was added to water (0.5 mM) and sonicated for 1 h, during which surfactant-like behavior such as bubble generation was observed upon vigorous shaking (the photo in Fig. 1). This prompted us to perform DLS of the solution, which revealed that the solution contained colloids with diameters ranging from 70 to 700 nm (average of 320 nm) (Fig. 3A). Further drop shape analyses as a function of solution concentration revealed a critical assembly concentration of *ca*. 0.03 mM, indicating a notable decrease in surface tension (Fig. S3). Furthermore, TEM experiments (Fig. 3B) and dye entrapment and release experiments (Fig. S5) revealed spherical hollow structures as vesicles, thus indicating that tACB[7] self-assembled into vesicles in water. Upon subjecting the solution to repeated extrusions through a 100 nm-pore membrane, the average diameter of the colloids decreased to 110 nm with a narrower size distribution, as confirmed by DLS (Fig. 3C). Despite the change in diameter, the particles remained hollow morphology with approximately 5 nm membrane thickness, as evidenced by TEM (Fig. 3D and S4). These results illustrate that tACB[7] spontaneously

forms vesicular membranes in water. These membranes can be reorganized upon applying mechanical forces, resulting in uniformly sized vesicles and thereby demonstrating the size tunability of vesicles formed with *t*ACB[7] (*i.e.,* *t*ACB[7] vesicles). Despite the ability of *t*ACB[7] to form vesicles due to its apparent amphiphilic nature, accurately characterizing its structural configuration in the membrane remains highly challenging owing to the concurrent presence of randomly coexisting hydrophilic and hydrophobic groups on its periphery and hydrophilic carbonyl-lined portals.

Given the previous reports on unconventional amphiphiles that have ambiguous structural features to define hydrophilic and hydrophobic units, yet function as building blocks for self-assembly (*e*.g., amphiphilic hyperbranched polymers and macrocyclic molecules with multiple arms) [15,37], this CB[7]-based amphiphile seems to align with this unconventional category. Thus, this study illustrates an approach to confer amphiphilicity to CB[7] through synthetic design, serving as a guiding pathway for the development of a new class of unconventional amphiphiles bearing a functional macrocycle.

3.3. *Host–guest interactions of tACB[7] vesicles*

With *t*ACB[7] vesicles, accessibility of the CB[7] portal on the vesicles was examined by utilizing TIRF microscopy in conjunction with fluorescein isothiocyanate conjugated adamantylamine (FITC-AdA, Fig. 4A) [24]. This approach used the high-affinity binding of AdA to CB[7] (with a binding constant, $K_a \sim 10^{13}$ M^{-1}) [6], known to be a non-covalent version of clicking pair system [38]. It has been previously reported that peripheral functionalization of CB[7] has no significant impact on its binding affinity to guests, which is attributed to the structural rigidity of the CB[7] motif. [11,13,39], thus, the AdA and CB[7] derivatives still exhibit high-affinity binding as they recognize each other very efficiently and selectively under various biological conditions, including cell culture media, cytosol, and the bloodstream, thereby serving as supramolecular lathing system for bioimaging and protein isolation [40–43]. The vesicles were treated with FITC-AdA for 6 h, followed by overnight dialysis against water using a RC membrane (MWCO 3.5 kDa). The resulting solution exhibited a 4-nm red-shifted emission band compared to that of the free FITC-AdA (Fig. S6). In the resulting solution, fluorescent dots were clearly visualized using TIRF in the green channel, corresponding to the FITC signal (Fig. 4B). A control experiment was conducted with carboxyfluorescein (CF), which hardly interacts with CB[7] in water, unlike FITC-AdA (Fig. S7: no chemical shift in the CF protons even after CB[7] treatment in D_2O). No apparent fluorescent signal was detected from the solution of the *t*ACB[7] vesicles after dialysis. Such a result indicates the insufficient charge-charge interaction between CF and the surface of the *t*ACB[7] vesicles to retain CF on the vesicles. Moreover, it clearly highlights the importance of the AdA moiety for the introduction of FITC-AdA into the vesicles via host–guest interactions between AdA and the CB[7] motif, being in agreements with previous reports using dye-AdA and CB[7] derivatives [29,42,44–48].

This result also confirms the accessibility of the CB[7] portal on the vesicles for guest binding. In addition, despite treating the vesicle with 2-fold excess amount of a guest molecule such as *N*-(1-adamantyl)ethylenediammonium, known for notably higher binding affinity to CB[7] ($K_a \sim 10^{15}$ M^{-1})[6] compare to any ammonium aliphatic motifs ($K_a \sim 10^3$ - 10^7 M^{-1}), [6] the vesicle size remained unaltered for a week long observation, as confirmed by DLS analysis. This observation suggests that the intermolecular interaction between the *tert*–ammonium arms and the CB[7] portal lacks significant influence on the structural integrity or size of the vesicles. This limited impact of the ammonium arms likely results from their inability to fit well within the CB[7] cavity due to their short carbon chain length and their congested locations on the periphery of the CB[7] derivative. Thus, it indicates the durability of the vesicle membrane even after treatment with guest molecules for at least a week, which is long enough to demonstrate the potential of *t*ACB[7] vesicles for drug delivery.

In addition, although the molecular-level structure of the vesicular membranes still remains unclear, the observed membrane thickness and the accessibility of molecular cavities on the surface for host–guest interactions provide clues for proposing a plausible model of the membrane. The *t*ACB[7] molecules form a layer with their arms aligned parallel to the vesicular layer with their carbonyl-rimmed portals of *t*ACB[7] oriented outward toward water. Approximately five such layers stack together to form the stable vesicle membrane. The portals in the outermost layer remain accessible to guest molecules, enabling host–guest interactions.

3.4. *Intracellular behavior of tACB[7] vesicles and drug delivery potential*

With the vesicles having stable membrane structure, the intracellular behavior of the vesicles was explored. *In vitro* cell experiments were conducted using HeLa cells, an established model of human cervical carcinoma. In the experimental design, FITC-AdA was found to be useful for reliable vesicle tracking using fluorescence imaging. Confocal laser scanning microscopy (CLSM), shown in Fig. 4C, displayed pronounced green fluorescence signals in the cytosol of cells in the FITC channel when the cells were treated with FITC-AdA coated *t*ACB[7] vesicles (FITC-AdA@*t*ACB[7] vesicles). This effect was more evident in the magnified images of the cells (Fig. 4E). In the control cell experiment using only FITC-AdA without *t*ACB[7] vesicles, no efficient intracellular uptake was observed, with an almost negligible fluorescence signal within the cells in the CLSM images (Fig. 4D). This illustrates the internalization of *t*ACB[7] vesicles into cancer cells. Subsequently, we measured the zeta-potential of the vesicles with OxPt to be 18 ± 2 mV (Fig. S13). These results suggest that the positively charged surface of the vesicles, resulting from the presence of ammonium groups on *t*ACB[7], likely plays a role in facilitating cellular uptake, given that the positive surface charge of nanomaterials can enhance cellular uptake by interacting with plasma membranes and associated proteins [49–52].

In addition to an AdA derivative with exceptionally high affinity for CB[7], the internalization of a spermine (SPM) derivative, FITC-conjugated spermine (FITC-SPM) [15], was

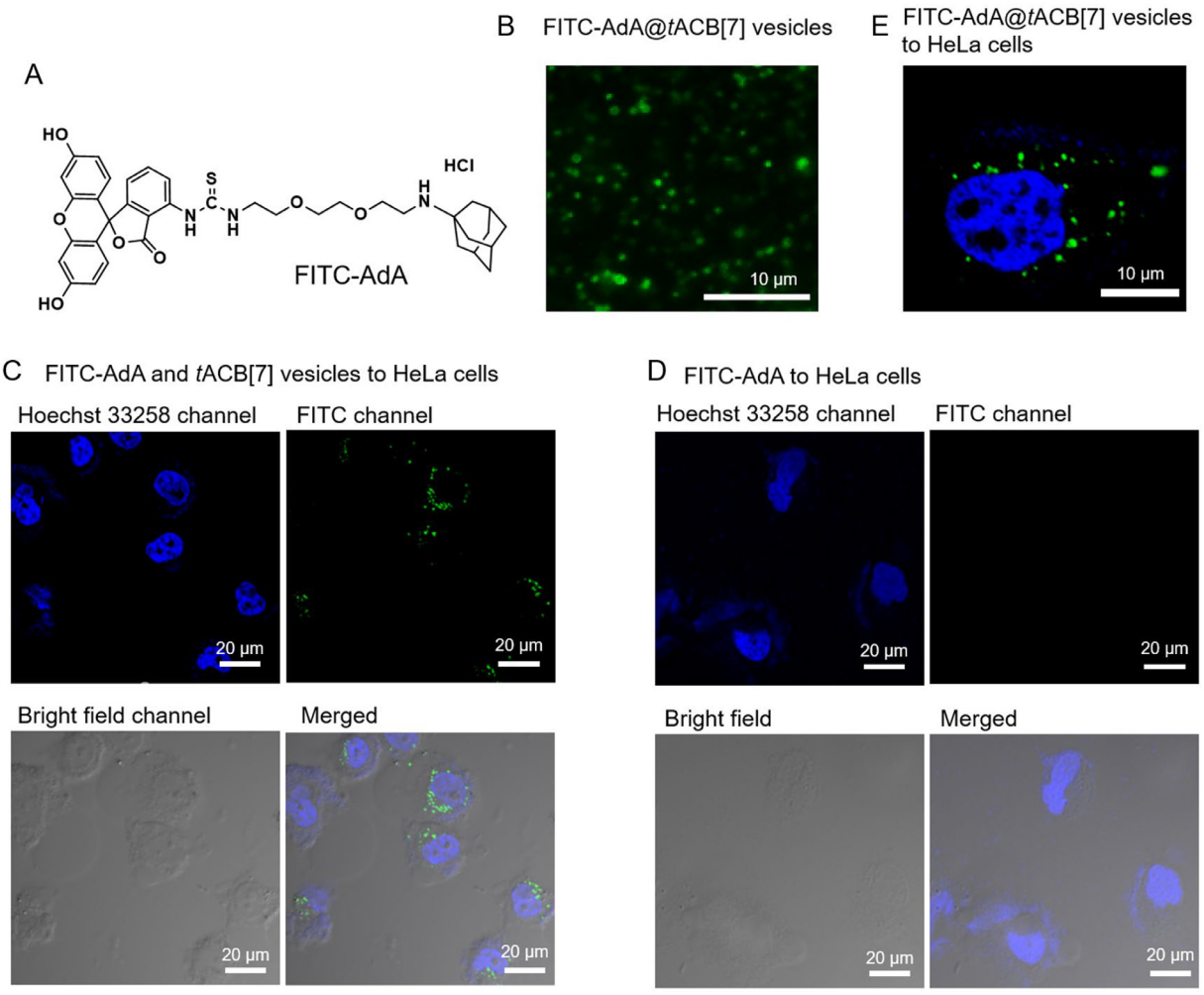

Fig. 4 – (A) Chemical structure of FITC-AdA. (B) TIRF image of the FITC-AdA@tACB[7] vesicles. (C-E)Confocal laser scanning microscopy image of HeLa cells treated with (C) FITC-AdA@tACB[7] vesicles, (D) FITC-AdA, and (E) enlarged image of HeLa cells treated with FITC-AdA@tACB[7] vesicles. The blue (Hoechst 33,258 channel) and green (FITC channel) images were taken at an excitation of 408 and 488 nm for visualization of the nucleus and tACB[7] vesicles, respectively.

also observed upon treatment of cells with tACB[7] vesicles (Fig. S8). SPM has a lower binding affinity to CB[7] compared with AdA (K_a of SPM to CB[7] is 1.2×10^6 M^{-1} [34], which is several orders less than that of AdA to CB[7]). Given the similarity in binding affinity between SPM and OxPt to CB[7] (K_a of OxPt to CB[7] is 2.8×10^6 M^{-1}) [32–34], enhanced uptake of OxPt into cancer cells with tACB[7] vesicles was hypothesized, analogous to the behavior of FITC-SPM. To examine this, cytotoxicity of OxPt and tACB[7] vesicles or both to HeLa cells was measured using the MTT (3-[4,5-dimethylthiazol-2-yl]−2,5 diphenyl tetrazolium bromide) assay. MTT assay of tACB[7] vesicles revealed that <10 μM of tACB[7] is not severely cytotoxic as confirmed by detecting >90% cell viability (Fig. S9). In addition, the results of the cell experiments showed a reduced cytotoxicity of OxPt when co-treated with CB[7] (Fig. S10), which is consistent with previous reports[34–35]. This reduction is possibly due to either the diminished cellular uptake or reduced cytotoxicity of OxPt upon complex formation with CB[7], or a combination of both. Conversely, treatment of OxPt combined with the tACB[7] vesicles resulted in an enhanced anti-cancer efficiency compared to treatment with CB[7]. Such results can be attributed to the host-guest interactions of the drug with the CB[7] portals in the tACB[7] vesicles (Fig. S11), as well as the nanosized features of the tACB[7] vesicles with their positive surface charge (DLS and zeta potential measurements in Fig. S12 and S13, respectively). Furthermore, the vesicles kept their morphology intact even when combined with OxPt (TEM image in Fig. S14), facilitating the efficient internalization of the nanomaterial with the drug into the cancer cells. This result clearly shows the potential of CB[7] derivatives capable of self-assembling into nanocolloids for drug delivery.

4. Conclusions

Employing thiol-ene photoreactions, hydrophilic *tert*–ammonium units are conjugated to the periphery of a non-water-soluble CB[7] derivative, resulting in the synthesis

of tACB[7], a new CB[7]-based amphiphile that self-assembles into tACB[7] vesicles. Capitalizing on the synergistic effect of both the nanostructured architecture with a positive surface charge and the unique host–guest chemistry of CB[7], particularly with anticancer drugs like OxPt, these vesicles demonstrated effective internalization into cells with OxPt and showed the enhanced cytotoxicity of the drug against cancer cells. Moreover, this study gives insights into designing new CB[7] derivatives, envisioning a diverse spectrum of amphiphiles potentially achievable by introducing various hydrophilic functionalities through well-established thiol-ene photoreactions. Thus, this work highlights a guide for a novel category of amphiphiles, and showcases the potential of the macrocycle-based amphiphiles forming nano-assemblies for biomedical applications such as drug delivery.

Conflicts of interest

The author reports no conflicts of interest.

Acknowledgment

This work was supported by the National Research Foundation of Korea [NRF-2023–00211758]. We thank Dr. A. Lee and Dr. Y. H. Ko for their helpful support and discussion on ESI-MS and NMR analysis.

Supplementary materials

Supplementary material associated with this article can be found, in the online version, at doi:10.1016/j.ajps.2024.101014. The figures and tables with "S" before the serial number are included in the Supplementary material.

References

[1] Murray J, Kim K, Ogoshi T, Yao W, Gibb BC. The aqueous supramolecular chemistry of cucurbit[*n*]urils, pillar[*n*]arenes and deep-cavity cavitands. Chem Soc Rev 2017;46(9):2479–96.
[2] Liu Z, Nalluri SKM, Stoddart JF. Surveying macrocyclic chemistry: from flexible crown ethers to rigid cyclophanes. Chem Soc Rev 2017;46(9):2459–78.
[3] Jie K, Zhou Y, Yao Y, Huang F. Macrocyclic amphiphiles. Chem Soc Rev 2015;44(11):3568–87.
[4] Lagona J, Mukhopadhyay P, Chakrabarti S, Isaacs L. The cucurbit[*n*]uril family. Angew Chem Int Ed 2005;44(31):4844–70.
[5] Masson E, Ling XX, Joseph R, Kyeremeh-Mensah L, Lu XY. Cucurbituril chemistry: a tale of supramolecular success. RSC Adv 2012;2(4):1213–47.
[6] Barrow SJ, Kasera S, Rowland MJ, del Barrio J, Scherman OA. Cucurbituril-based molecular recognition. Chem Rev 2015;115(22):12320–406.
[7] Assaf KI, Nau WM. Cucurbiturils: from synthesis to high-affinity binding and catalysis. Chem Soc Rev 2015;44(2):394–418.
[8] Cheng G, Luo J, Liu Y, Chen X, Wu Z, Chen T. Cucurbituril-oriented nanoplatforms in biomedical applications. ACS Appl Bio Mater 2020;3(12):8211–40.
[9] Kim K, Selvapalam N, Ko YH, Park KM, Kim D, Kim J. Functionalized cucurbiturils and their applications. Chem Soc Rev 2007;36(2):267–79.
[10] Lucas D, Minami T, Iannuzzi G, Cao L, Wittenberg JB, Anzenbacher P, et al. Templated synthesis of glycoluril hexamer and monofunctionalized cucurbit[6]uril derivatives. J Am Chem Soc 2011;133(44):17966–76.
[11] SY Jon, Selvapalam N, Oh DH, Kang JK, Kim SY, Jeon YJ, et al. Facile synthesis of cucurbit[*n*]uril derivatives via direct functionalization: expanding utilization of cucurbit[*n*]uril. J Am Chem Soc 2003;125(34):10186–7.
[12] Zhao N, Lloyd GO, Scherman OA. Monofunctionalised cucurbit[6]uril synthesis using imidazolium host–guest complexation. Chem Commun 2012;48(25):3070–2.
[13] Dong N, He J, Li T, Peralta A, Avei MR, Ma M, et al. Synthesis and binding properties of monohydroxycucurbit[7]uril: a key derivative for the functionalization of cucurbituril hosts. J Org Chem 2018;83(10):5467–73.
[14] Park KM, Hur MY, Ghosh SK, Boraste DR, Kim S, Kim K. Cucurbit[*n*]uril-based amphiphiles that self-assemble into functional nanomaterials for therapeutics. Chem Commun 2019;55(72):10654–64.
[15] Lee H-K, Park KM, Jeon YJ, Kim D, Oh DH, Kim HS, et al. Vesicle formed by amphiphilc cucurbit[6]uril: versatile, noncovalent modification of the vesicle surface, and multivalent binding of sugar-decorated vesicles to lectin. J Am Chem Soc 2005;127(14):5006–7.
[16] Park KM, Suh K, Jung H, Lee DW, Ahn Y, Kim J, et al. Cucurbituril-based nanoparticles: a new efficient vehicle for targeted intracellular delivery of hydrophobic drugs. Chem Commun 2009;2009(1):71–3.
[17] Park KM, Lee DW, Sarkar B, Jung H, Kim J, Ko YH, et al. Reduction-sensitive, robust vesicles with a non-covalently modifiable surface as a multifunctional drug-delivery platform. Small 2010;6(13):1430–41.
[18] Huang WH, Zavalij PY, Isaacs L. Cucurbit[*n*]uril formation proceeds by step-growth cyclo-oligomerization. J Am Chem Soc 2008;130(26):8446–54.
[19] Jiao D, Zhao N, Scherman OA. A "green" method for isolation of cucurbit[7]uril via a solid state metathesis reaction. Chem Commun 2010;46(12):2007–9.
[20] Wu F, Wu LH, Xiao X, Zhang YQ, Xue SF, Tao Z, et al. Locating the cyclopentano cousins of the cucurbit[*n*]uril family. J Org Chem 2012;77(1):606–11.
[21] Vinciguerra B, Cao L, Cannon JR, Zavalij PY, Fenselau C, Isaacs L. Synthesis and self-assembly processes of monofunctionalized cucurbit[7]uril. J Am Chem Soc 2012;134(31):13133–40.
[22] Ayhan MM, Karoui H, Hardy M, Rockenbauer A, Charles L, Rosas R, et al. Comprehensive synthesis of monohydroxy-cucurbit[*n*]urils ($n = 5, 6, 7, 8$): high purity and high conversions. J Am Chem Soc 2015;137(32):10238–45.
[23] Ghosh SK, Dhamija A, Ko YH, An J, Hur MY, Boraste DR, et al. Superacid-mediated functionalization of hydroxylated cucurbit[*n*]urils. J Am Chem Soc 2019;141(44):17503–6.
[24] Park KM, Baek K, Ko YH, Shrinidhi A, Murray J, Jang WH, et al. Mono-allyloxylated cucurbit[7]uril acts as an unconventional amphiphile to form light-responsive vesicles. Angew Chem Int Ed 2018;57(12):3132–6.
[25] Park KM. Self-sorted compartmentalization by simultaneous use of natural and synthetic amphiphiles. Chem Asian J 2021;16(22):3645–8.
[26] Chen J, Li S, Wang Z, Pan Y, Wei J, Lu S, et al. Synthesis of an aiegen functionalized cucurbit[7]uril for subcellular bioimaging and synergistic photodynamic therapy and supramolecular chemotherapy. Chem Sci 2021;12(22):7727–34.
[27] Wang Z, Sun C, Wang R. Macrocycle-surfaced polymer

nanocapsules: an emerging paradigm for biomedical applications. Bioconjugate Chem 2022;33(12):2254–61.
[28] Cheng Q, Li S, Sun C, Yue L, Wang R. Stimuli-responsive perallyloxycucurbit[6]uril-based nanoparticles for selective drug delivery in melanoma cells. Mater Chem Front 2019;3(2):199–202.
[29] Sun C, Zhang H, Li S, Zhang X, Cheng Q, Ding Y, et al. Polymeric nanomedicine with "lego" surface allowing modular functionalization and drug encapsulation. ACS Appl Mater Inter 2018;10(30):25090–8.
[30] Das D, Assaf KI, Nau WM. Applications of cucurbiturils in medicinal chemistry and chemical biology. Front Chem 2019;7:619.
[31] Liu YH, Zhang YM, Yu HJ, Liu Y. Cucurbituril-based biomacromolecular assemblies. Angew Chem Int Ed 2021;60(8):3870–80.
[32] Jeon YJ, Kim SY, Ko YH, Sakamoto S, Yamaguchi K, Kim K. Novel molecular drug carrier: encapsulation of oxaliplatin in cucurbit[7]uril and its effects on stability and reactivity of the drug. Org Biomol Chem 2005;3(11):2122–5.
[33] Wu H, Chen H, Tang B, Kang Y, Xu JF, Zhang X. Host–guest interactions between oxaliplatin and cucurbit[7]uril/cucurbit[7]uril derivatives under pseudo-physiological conditions. Langmuir 2020;36(5):1235–40.
[34] Chen Y, Huang Z, Zhao H, Xu JF, Sun Z, Zhang X. Supramolecular chemotherapy: cooperative enhancement of antitumor activity by combining controlled release of oxaliplatin and consuming of spermine by cucurbit[7]uril. ACS Appl Mater Inter 2017;9(10):8602–8.
[35] Cao L, Hettiarachchi G, Briken V, Isaacs L. Cucurbit[7]uril containers for targeted delivery of oxaliplatin to cancer cells. Angew Chem Int Ed 2013;52(46):12033–7.
[36] Rotenberg Y, Boruvka L, Neumann AW. Determination of surface tension and contact angle from the shapes of axisymmetric fluid interfaces. J Colloid Interface Sci 1983;93(1):169–83.
[37] Jiang W, Zhou Y, Yan D. Hyperbranched polymer vesicles: from self-assembly, characterization, mechanisms, and properties to applications. Chem Soc Rev 2015;44(12):3874–89.
[38] Schreiber CL, Smith BD. Molecular conjugation using non-covalent click chemistry. Nat Rev Chem 2019;3(6):393–400.
[39] Hwang I, Baek K, Jung M, Kim Y, Park KM, Lee DW, et al. Noncovalent immobilization of proteins on a solid surface by cucurbit[7]uril-ferrocenemethylammonium pair, a potential replacement of biotin−avidin pair. J Am Chem Soc 2007;129(14):4170–1.
[40] Li M, Lee A, Kim KL, Murray J, Shrinidhi A, Sung G, et al. Autophagy caught in the act: a supramolecular fret pair based on an ultrastable synthetic host–guest complex visualizes autophagosome–lysosome fusion. Angew Chem Int Ed 2018;57(8):2120–5.
[41] Li M, Kim S, Lee A, Shrinidhi A, Ko YH, Lim HG, et al. Bio-orthogonal supramolecular latching inside live animals and its application for *in vivo* cancer imaging. ACS Appl Mater Inter 2019;11(47):43920–7.
[42] Kim KL, Sung G, Sim J, Murray J, Li M, Lee A, et al. Supramolecular latching system based on ultrastable synthetic binding pairs as versatile tools for protein imaging. Nat Commun 2018;9(1):1712.
[43] An J, Kim S, Shrinidhi A, Kim J, Banna H, Sung G, et al. Purification of protein therapeutics via high-affinity supramolecular host–guest interactions. Nat Biomed Eng 2020;4(11):1044–52.
[44] Sasmal R, Das Saha N, Pahwa M, Rao S, Joshi D, Inamdar MS, et al. Synthetic host–guest assembly in cells and tissues: fast, stable, and selective bioorthogonal imaging via molecular recognition. Anal Chem 2018;90(19):11305–14.
[45] Zou L, Braegelman AS, Webber MJ. Spatially defined drug targeting by *in situ* host–guest chemistry in a living animal. ACS Cent Sci 2019;5(6):1035–43.
[46] Yin H, Cheng Q, Bardelang D, Wang R. Challenges and opportunities of functionalized cucurbiturils for biomedical applications. JACS Au 2023;3(9):2356–77.
[47] Sim J, Lee A, Kim D, Kim KL, Park B-J, Park KM, et al. A combination of bio-orthogonal supramolecular clicking and proximity chemical tagging as a supramolecular tool for discovery of putative proteins associated with laminopathic disease. Small 2023;19(21):2208088.
[48] Lee A, Sung G, Shin S, Lee S-Y, Sim J, Nhung TTM, et al. Orthoid: profiling dynamic proteomes through time and space using mutually orthogonal chemical tools. Nat Commun 2024;15(1):1851.
[49] Harush-Frenkel O, Rozentur E, Benita S, Altschuler Y. Surface charge of nanoparticles determines their endocytic and transcytotic pathway in polarized mdck cells. Biomacromolecules 2008;9(2):435–43.
[50] Dausend J, Musyanovych A, Dass M, Walther P, Schrezenmeier H, Landfester K, et al. Uptake mechanism of oppositely charged fluorescent nanoparticles in hela cells. Macromol Biosci 2008;8(12):1135–43.
[51] Sousa de Almeida M, Susnik E, Drasler B, Taladriz-Blanco P, Petri-Fink A, Rothen-Rutishauser B. Understanding nanoparticle endocytosis to improve targeting strategies in nanomedicine. Chem Soc Rev 2021;50(9):5397–434.
[52] He C, Hu Y, Yin L, Tang C, Yin C. Effects of particle size and surface charge on cellular uptake and biodistribution of polymeric nanoparticles. Biomaterials 2010;31(13):3657–66.